NANO · MICRO small
www.small-journal.com

Adsorbed Carbon Monoxide-Enabled Self-Terminated Au-Grafting on Pt_6 Nanoclusters for Enhanced Methanol Electrooxidation

*Paloli Mymoona, Edakkattuparambil Sidharth Shibu, and Chinnaiah Jeyabharathi**

C.J. dedicates this article to Dr. Kanala Lakshminarasimha Phani, Chief Scientist (retired), CSIR-CECRI for his mentorship.

The study presents the first example of an adsorbed carbon monoxide (CO) enabled self-terminated Au-grafting on triphenylphosphine (PPh_3) stabilized Pt_6 nanoclusters (NCs) (Pt_6 $(PPh_3)_4Cl_5$ NCs or Pt_6 NCs). Adsorbed PPh_3 ligands weaken the Pt-CO bond enabling the self-terminated Au-grafting on Pt_6 NCs. The Au-grafted Pt_6 NCs exhibit enhanced methanol electrooxidation (MOR) in acidic solutions. The surface is composed of a PtAu ensemble exhibiting enhanced MOR and CO tolerance due to the synergistic interaction of Pt with Au and PPh_3. The hydrogen underpotential deposition (H-UPD) signal from a CO-covered surface reveals the existence of free-Pt sites on the PtAu ensemble causing higher MOR reactivity. The Au and PPh_3 ensure electrocatalytic activity of the NCs, depriving of them at anodic potentials results in "*a death-valley*" trend.

1. Introduction

The property of the electrocatalysts towards oxygen reduction (ORR) and methanol electrooxidation (MOR) relies on their surface electronic structure, which can be tuned by ligand, strain, and geometric effect.[1] Bimetallic systems exhibit a synergistic effect to enhance the reactivity of MOR. This can be achieved by tuning the surface ensemble structures favoring the reactivity.[1a,b,2] Here, dealloying, surface segregation, underpotential deposition, etc. are a few proven strategies to tune the surface that enhances the catalytic activity of Pt-based electrocatalysts.[3] Because of the interaction between Pt and non-Pt metals (ligand effect), not only the catalytic activity is enhanced greatly but also the usage of Pt metal is notably decreased. Alloying Au with Pt has been shown to work synergistically to enhance MOR reactivity. Although, Au is inert in the bulk state, supported Au nanoparticles (NPs) exhibit high catalytic activity for room-temperature oxidation of carbon monoxide (CO).[4] Considering the MOR, Au is not catalytic in acid electrolytes. But, its stabilization effect and electronic interaction over Pt significantly enhance both the electrocatalytic MOR activity and stability of AuPt NPs.[5] Despite the promising reactivity of metal and alloy NP electrocatalysts, the mass loading of the active metals in them is so high on top of the inherent challenges associated with control over the size, shape, dispersity, surface structure, and composition.[6] Alternatively, atomically precise noble metal nanoclusters (NCs) can be synthesized with definite metal-core size and surface functionality, which serves as a bridge between single metal atoms and NPs, and exhibits distinctively different reactivity owing to ultrasmall size (<2 nm), high surface-to-volume-ratio, well-defined atomic precision structure, and diverse surface functionalities and physicochemical properties, such as luminescence, chirality, and quantum confinement.[7] These distinctive characteristics have positioned metal NCs as valuable tools for addressing a wide range of challenges in various fields. In particular, metal NCs have found utility as model catalysts for significant electrochemical reactions such as carbon dioxide reduction reaction (CO_2RR), water splitting reactions (hydrogen evolution reaction (HER) and oxygen evolution reaction (OER)), alcohol oxidation, oxygen reduction reaction (ORR), etc.[8] This usage has paved the way to explore new strategies for improving catalytic efficiency of molecular nano-catalysts, their stability, and selectivity. However, the reactivity of NCs is hindered by strongly adsorbed ligands, limiting their full potential as an electrocatalyst.[9] However, ligands like triphenylphosphine (PPh_3) were shown not to affect the reactivity of Pt NPs for ORR.[10] This makes it possible to design better electrocatalysts without resorting to aggregation and coalescence and retain reactivity and stability of the NCs, which is a stumbling block in NP electrocatalysts.

P. Mymoona, C. Jeyabharathi
Council of Scientific and Industrial Research (CSIR)-Central
Electrochemical Research Institute (CECRI)
Karaikudi, Tamil Nadu 630003, India
E-mail: cjeyabharathi@cecri.res.in

P. Mymoona, C. Jeyabharathi
Academy of Scientific and Innovative Research (AcSIR)
Ghaziabad 201002, India

E. S. Shibu
Smart Materials Lab
Department of Nanoscience and Technology (DNST)
University of Calicut (UoC)
Malappuram, Kerala 673635, India

The ORCID identification number(s) for the author(s) of this article can be found under https://doi.org/10.1002/smll.202401998

DOI: 10.1002/smll.202401998

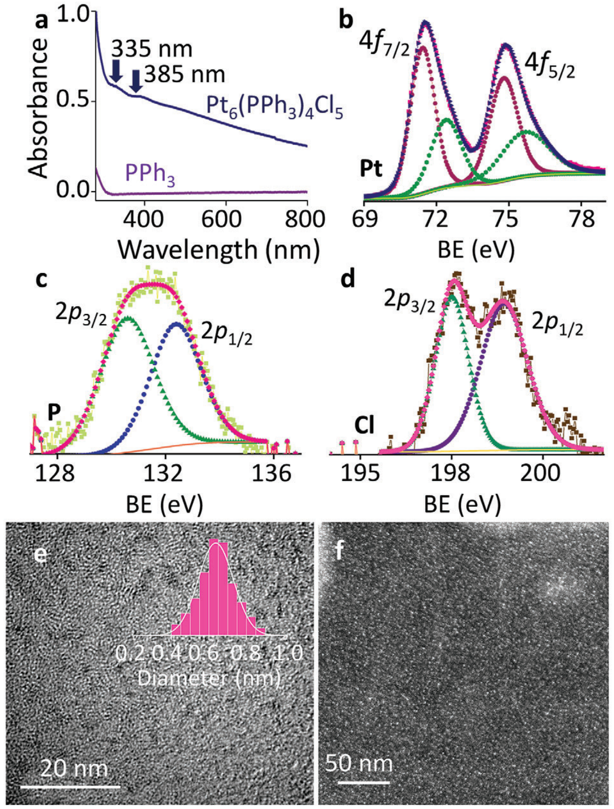

Figure 1. a) UV–vis absorption spectra of Pt_6 NCs. XPS spectra for b) Pt 4*f*, c) P 2*p*, and d) Cl 2*p* of Pt_6 NCs. e) HR-TEM and f) HAADF-STEM images of Pt_6 NCs with size distribution.

Moreover, nanocatalysts experience degradation at high anodic potentials, particularly Pt, which can be suppressed by decorating the surface with noble metals like Au.[5,11] Exploiting this property of Au in stabilizing Pt in addition to the possible synergistic effect between Au and Pt at the atomic-cluster level, we synthesized Pt_6 NCs stabilized by PPh_3 and modified them with Au atoms in a self-terminative fashion enabled by adsorbed carbon monoxide (CO_{ads}). The grafting of Au on Pt_6 NCs using CO_{ads} is due to an anomalous behavior of the Pt-CO bond to reduce the Au^{3+} to obtain Au@Pt_6 NCs, which was not the case with Pt NPs. This is due to the strong Pt-CO bond in NP contrary to the weak Pt-CO bond in Pt_6 NCs. The resulting Au-grafted Pt_6 NCs exhibited improved stability, enhanced electrocatalytic activity of MOR, and CO tolerance than Pt_6 NCs and Pt/C in acidic solutions.

2. Results and Discussion

2.1. Synthesis and Characterization of Pt_6 NCs

The Pt_6 NCs were synthesized as in ref. [12] with some modifications (Figure S1, Supporting Information, and Experimental details, Supporting Information section). The Pt_6 NCs formation was confirmed through absorption bands at 335 and 385 nm, which is absent in the PPh_3 ligand (**Figure** 1a). The core size and composition of Pt_6 NCs were analyzed using matrix-assisted laser desorption/ionization time-of-flight (MALDI-TOF) mass spectrometry, as illustrated in Figure S2 (Supporting Information). The molecular ion peak at *ca*. 1876 Da corresponds to the species $Pt_6(PPh_3)_2Cl_5$ with a charge of +1 as assessed from the isotopic pattern (inset of Figure S2, Supporting Information). This molecular ion peak is 520 Da lower than the calculated mass of $Pt_6(PPh_3)_4Cl_5$ NCs, which is 2396 Da. The reduction in mass corresponds to the mass of two PPh_3 molecules, which might have been lost due to facile dissociation during ionization of the clusters upon MADLI-TOF measurements, which is a commonly observed effect.[13] The X-ray Photoelectron Spectrum (XPS) of Pt_6 NC exhibited binding energies (BE) at 71.28 ($4f_{7/2}$) and 74.66 eV ($4f_{5/2}$) for Pt^0 and at 72.02 eV ($4f_{7/2}$) and 75.26 eV ($4f_{5/2}$) for Pt^{2+} (Figure 1c). Also, P 2*p* (Figure 1d) and Cl 2*p* (Figure 1e) states at 130.82 eV (P $2p_{3/2}$), 132.60 eV (P $2p_{1/2}$), 198.04 eV (Cl $2p_{3/2}$), and 199.73 eV (Cl $2p_{1/2}$) were observed confirming the existence of PPh_3 and chlorides on the NCs. Further, the Pt_6 NCs were impregnated on Vulcan XC-72 carbon for electrochemical studies. The XPS of Pt_6 NC/C (Figure S3, Supporting Information) shows the spin-orbit doublet peaks with BE Pt^0 at 71.39 ($4f_{7/2}$) and 74.77 eV ($4f_{5/2}$) and of Pt^{2+} at 72.48 eV ($4f_{7/2}$) and 75.98 eV ($4f_{5/2}$). The observed peaks correspond to P 2*p* and Cl 2*p* states at 130.82 eV (P $2p_{3/2}$), 132.60 eV (P $2p_{1/2}$), 198.04 eV (Cl $2p_{3/2}$), and 199.73 eV (Cl $2p_{1/2}$) which are comparable to pristine Pt_6 NC. The Pt_6 NCs (0.65 ± 0.25 nm; Figure 1e) were uniformly distributed as assessed from High Resolution-Transmission Electron Microscopy (HR-TEM). The corresponding High-Angle Annular Dark-Field Scanning Transmission Electron Microscopy (HAADF-STEM) image is provided in Figure 1f, where the innumerous tiny bright spots are due to the NCs. The elemental mapping of the Pt_6 NC confirms the uniform distribution of Pt, P, and Cl (Figure S4a–d, Supporting Information). The Pt_6 NCs are immobilized over carbon support and studied microscopically. The HR-TEM, HAADF-STEM and EDS elemental mapping of Pt_6 NC/C (Figure S5a–f, Supporting Information) show the uniform distribution of the particles over carbon and confirm of the presence of Pt, P, and Cl. Due to the presence of carbon, the contrast was better and higher resolution was achieved even in bright field imaging.

2.2. Gold Grafting over Pt_6 NC/C and Testing CO Tolerance

The cyclic voltammograms (CV) (**Figure** 2a,b) curves of Pt_6 NC/C and Pt/C showed well-defined H-UPD adsorption/desorption and Pt oxidation/reduction peaks. Typically, UPD has been used as a probe reaction to study the surface structure. Since the driving force for the UPD process is the work function difference between the substrate and a dsorbate, any variation in surface structure (in turn surface energy) can be probed. Here, Pt_6 NC/C exhibited a negative shift in hydrogen desorption peaks at 0.104 and 0.173 V_{RHE} compared to Pt/C (0.122 and 0.210 V_{RHE}) (Figure S6, Supporting Information). This indicates the weaker hydrogen adsorption and thus lower oxidation potentials on Pt_6 NCs, suggesting a significant difference in surface electronic structure between Pt_6 NCs and Pt NPs.[12]

Additionally, CO-stripping voltammetry revealed that Pt_6 NC/C had lower onset (E_{onset} = 0.74 V_{RHE}) and peak potential (E_p = 0.89 V_{RHE}) for CO-oxidation compared to Pt/C (E_{onset} = 0.80 V_{RHE} and E_p = 0.90 V_{RHE}) (Figure 2c,d). This early

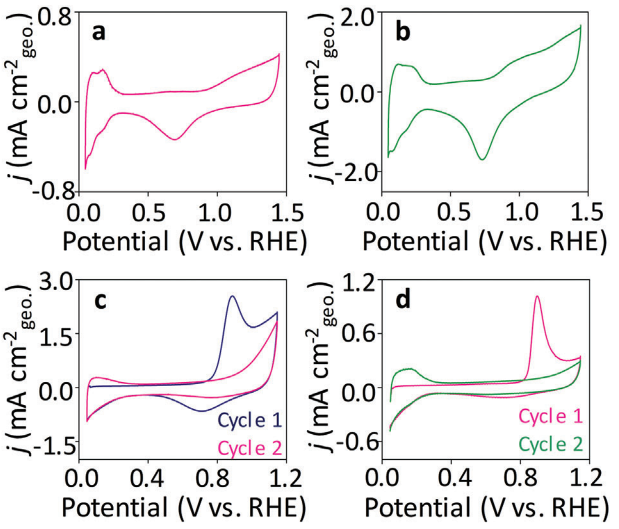

Figure 2. Cyclic voltammogram of a) Pt_6 NC/C and b) Pt/C and deaerated 0.1 м H_2SO_4 at 100 mV s^{-1}. CO-stripping curves of c) Pt_6 NC/C and d) Pt/C in deaerated 0.1 м H_2SO_4 at 50 mV s^{-1}.

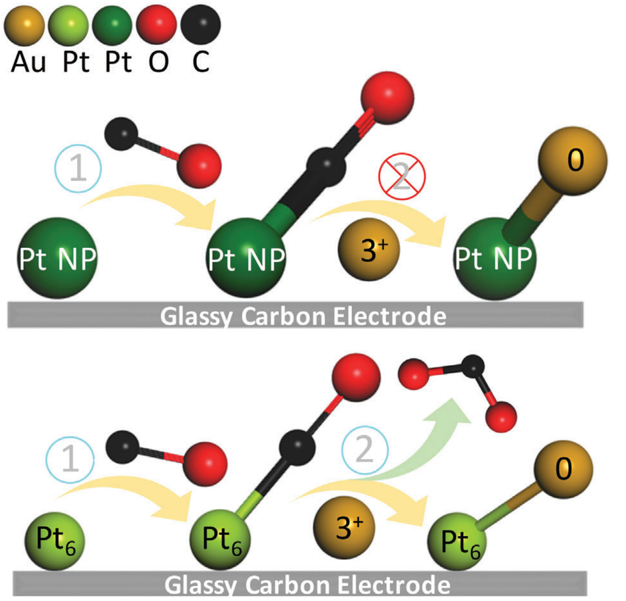

Figure 3. Schematic (non-stoichiometric) representation of Au-grafting on Pt_6 NC/C.

oxidation of CO_{ads} on Pt_6 NCs indicates the weaker Pt-CO bond strength and better CO-tolerance for Pt_6 NC/C than Pt/C. Xing et al. showed from DFT simulations that the Pt_6 NCs experienced a downshift in the d-band center based on the ligand effect imposed by the triphenylphosphine. The pristine Pt_6 NCs possessed lower CO adsorption strength (−1.1 eV) than that of Pt-NPs (−1.46 eV) and after the removal of triphenylphosphine by thermal annealing at 550 °C, they observed the stronger Pt-CO bond strength (−1.87 eV). Hence, weaker Pt-CO bond strength on Pt_6 NC/C makes it susceptible to oxidation by a strong oxidizing agent. Also, the CO molecule was used as the reducing agent to synthesize suspended Au_{22} NCs by reducing Au^{3+} ions, where CO_{ads} were shown to stabilize the Au-intermediates.[14] Since the Pt_{NP}-CO bond is strong, the CO oxidation would be difficult by Au^{3+} ions, whereas the weaker Pt_{NC}-CO_{ads} bond strength, as observed in our case, might facilitate the reduction of Au^{3+} to Au^0 (**Figure 3**). The voltammograms recorded after the immersion in 0.1 mм $HAuCl_4$ solution exhibited no CO stripping peak (Figure S7, Supporting Information), indicating the consumption of CO_{ads} for Au^{3+} reduction. Since the Au^{3+} reduction occured by pre-adsorbed CO on Pt sites, the Au decoration will be self-terminated once the CO_{ads} is consumed.

To confirm if Au is decorated over Pt_6 NC/C (Au@ Pt_6 NC/C), CV curves were recorded (**Figure 4a**). The CV of Au@Pt_6 NC/C showed an onset of Au oxidation at 1.29 V_{RHE} and a cathodic gold oxide reduction at 1.14 V_{RHE}, confirming the Au grafting on Pt_6 NC/C. Moreover, the platinum oxide reduction peak was shifted from 0.43 to 0.55 V_{RHE} signaling the geometric/ligand effect imposed by Au. An investigation into the surface decoration of Au on Pt_6 NC/C was conducted through the measurement of Open Circuit Voltage (OCV) across various interfaces. In Figure S8 (Supporting Information), the OCV values for Pt_6 NC/C, Pt_6 NC/C-CO_{ads}, Au@Pt_6 NC/C, and Pt_6 NC/C-CO_{ads} with the addition of $HAuCl_4$ to a 0.1 м H_2SO_4 during the experiment. The pristine Pt_6 NC/C exhibited an OCV of 0.57 $V_{Ag/AgCl}$. However, this value increased to 0.63 $V_{Ag/AgCl}$ and 0.69 $V_{Ag/AgCl}$ when the surface was modified with CO_{ads} and Au, respectively. Notably, the OCV of Pt_6 NC/C-CO_{ads} experienced a substantial enhancement when $HAuCl_4$ was introduced into the electrolyte, jumping from 0.63 $V_{Ag/AgCl}$ to 0.72 $V_{Ag/AgCl}$. This shift in OCV can be attributed to the alteration in the interfacial composition. The positive shift in the OCV value of Au@Pt_6 NC/C concerning Pt_6 NC/C indicates the chemical grafting of Au over exposed Pt sites. Furthermore, the broad Pb-UPD peak (0.0298 mC) at −0.14 $V_{Ag/AgCl}$ confirms the presence of Au sites (Figure S9, Supporting Information). Au grafting was unsuccessful on Pt/C due to a strong Pt_{NP}-CO bond (Figure S10, Supporting Information).

To check the CO tolerance, CO-stripping measurements were conducted (Figure 4b,c). Au@Pt_6 NC/C exhibited a weak and broad CO-oxidation wave, indicating that Au@Pt_6 NC/C can be a promising CO-tolerant MOR catalyst. To support this, an unusual H-UPD stripping feature (0.0415 mC) on a CO-covered surface was observed on Au@Pt_6 NC/C, which is absent in Pt_6 NC/C and Pt/C. This result suggests the existence of PtAu ensemble favoring on-top adsorption of CO without resorting to bridge and hollow type resulting in a weaker Pt-CO bond and adsorption of hydrogen in the neighboring Pt sites.

The XPS of Au@Pt_6 NC/C showed BE at 71.63 ($4f_{7/2}$) and 75.09 eV ($4f_{5/2}$) for Pt^0 and at 72.46 eV ($4f_{7/2}$) and 76.01 eV ($4f_{5/2}$) for Pt^{2+} (Figure 4d). Additionally, peaks at 84.05 ($4f_{7/2}$) and 87.68 eV ($4f_{5/2}$) were observed for Au^0 and at 85.30 eV ($4f_{7/2}$) and 89.00 eV ($4f_{5/2}$) for traces of Au^{1+}. This confirms the grafting of atomic Au on Pt_6 NCs (Figure 4e). The XPS of P 2*p* (Figure S11a, Supporting Information) and Cl 2*p* (Figure S11b, Supporting Information) was observed at 131.90 eV (P $2p_{3/2}$), 132.88 eV (P $2p_{1/2}$), 197.63 eV (Cl $2p_{3/2}$), and 199.41 eV (Cl $2p_{1/2}$), respectively confirms the comparable BE to pristine Pt_6 NC and Pt_6 NC/C. The similar core-level BE of Pt, P, and Cl along with Au suggests that the chemistry of the Pt_6 NCs is unaltered after Au grafting. The fraction of Au present in Au@Pt_6 NCs was evaluated by

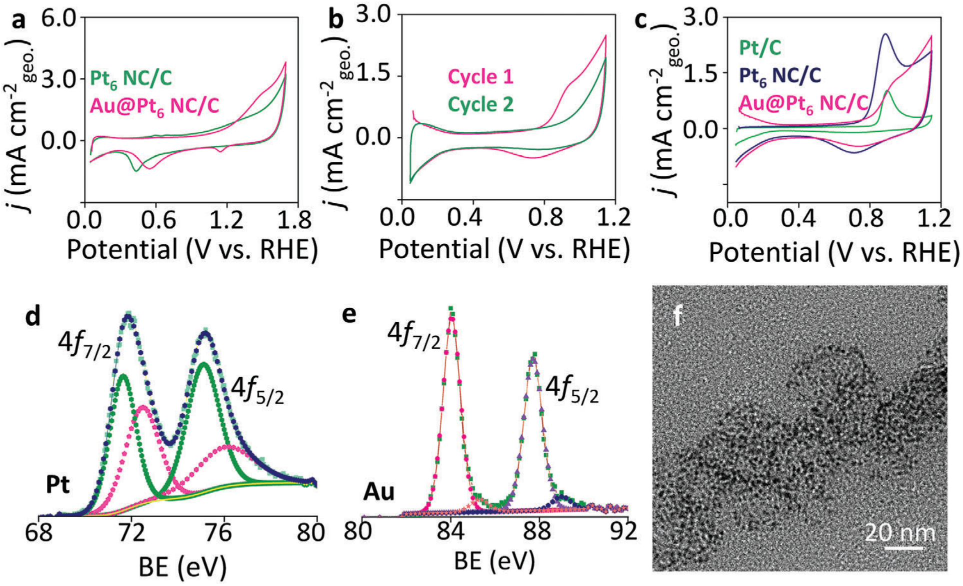

Figure 4. a) Cyclic voltammogram of Pt_6 NC/C and Au@Pt_6 NC/C in deaerated 0.1 м H_2SO_4 at 100 mV s^{-1}. CO-stripping curves of b) Au@Pt_6 NC/C and c) comparison with Pt_6 NC/C and Pt/C in deaerated 0.1 м H_2SO_4 at 50 mV s^{-1}. XPS of d) Pt 4*f* and e) Au 4*f*; and HR-TEM of Au@Pt_6 NC/C.

comparing the atomic percentage ratios of Au and Pt using the corresponding XPS data. This analysis involved assessing the normalized area of the XPS deconvoluted peaks. Normalization was performed using respective relative sensitivity factors (RSF) for the specific elements and electronic states (Table S1, Supporting Information). Using this approach to examine the XPS data, the atomic percentage ratio of Pt/Au in the Au@Pt_6 NCs is 5.7. These findings imply the ultralow loading of Au on the surface of Pt_6 NC/C and confirm the self-terminated Au decoration. In HR-TEM, the size distribution of the Au@Pt_6 NC/C has not changed appreciably (Figure 4f) and Au atoms are finely dispersed in the Au@Pt_6 NC/C as observed in elemental mapping (Figure S12, Supporting Information).

2.3. Electrocatalytic MOR Performance of Pt_6 NC/C and Au@Pt_6 NC/C

The MOR performances were performed using CV measurements. The Au@Pt_6 NC/C exhibited significantly improved MOR activity compared to Pt_6 NC/C and Pt/C. Au@Pt_6 NC/C exhibited a lower E_{onset} (0.39 V_{RHE}) along with higher specific (SA = 15.9 mA cm^{-2}) and mass activity (MA = 3149.40 mA mg_{Pt}^{-1}), compared to Pt_6 NC/C (E_{onset} = 0.48 $V_{\text{RHE,}}$ SA = 9.5 mA cm^{-2}, and MA = 1881.15 mA mg_{Pt}^{-1}) and Pt/C (E_{onset} = 0.58 V_{RHE}, SA = 3.7 mA cm^{-2}, and MA = 644. 74 mA mg_{Pt}^{-1}) (**Figure** 5a–c; Figure S13, Supporting Information). The MA of Au@Pt_6 NC/C was ca. 1.7 times higher than that of Pt_6 NC/C and ca. 4.9 times than Pt/C. This enhanced MOR reactivity is attributed to the inherent CO tolerance of Au@Pt_6 NC and can be rationalized due to the Pt—P and Pt—Au interaction. A shorter Pt—Pt bond length of NCs was reported due to the strong electronic coupling of Pt atoms with phosphine ligands.[10] Additionally, to assess the electrochemically active surface area (ECSA) of the catalysts CO-stripping voltammetry measurements were conducted. Details are given in the experimental section. Figure S14a–c (Supporting Information) illustrates the CO-stripping voltammogram of Pt/C, Pt_6 NC/C, and Au@Pt_6 NC/C, respectively. We derived the ECSA values for the prepared Pt/C, Pt6 NC/C, and Au@Pt6 NC/C catalysts using the CO-stripping measurements. The CO-stripping charge integration was performed after subtracting the integrated area of oxide reduction from the integrated area of CO oxidation. Through this approach, we isolated the charge specifically related to CO oxidation, excluding the possible Pt or Au surface oxidation charge. The high charge associated with oxide reduction observed in Pt_6 NC/C (144.2 µC) and Au@Pt_6 NC/C (78 µC) compared to Pt/C (17.94 µC) is likely due to the facile oxidation of CO on the NC surface, which initiates platinum oxidation. The reduction of Pt oxide occurs subsequently. The charge was used to calculate the ECSA employing a specific charge of 420 µC cm^{-2}. The calculated ECSAs for the Pt/C, Pt_6 NC/C, and Au@Pt_6 NC/C catalysts were determined as 0.2866, 0.9752, and 0.5186 cm^2, respectively. The ECSA was used to evaluate the specific activity by normalizing the MOR current with the ECSA and the ECSA normalized MOR curves are presented in Figure S14f (Supporting Information). The charge corresponding to oxide reduction and ECSA values are graphically depicted in a histogram (Figure S14d,e, Supporting Information) and the details are compiled in Table S2 (Supporting Information). The MOR curves normalized with the corresponding ECSA which is shown in Figure S14f (Supporting Information). The order of reactivity is Pt/C ~ Pt_6 NC/C < Au@Pt_6 NC/C. Electrochemical impedance spectroscopy (EIS) at 0.40 $V_{\text{Ag/AgCl}}$ Au@Pt_6 NC/C had 2.25 kΩ charge-transfer resistance (R_{ct}) compared to Pt_6 NC/C (9.93 kΩ) and Pt/C (24.69 kΩ) (Figure 5d). The lower R_{ct} suggests the accelerated MOR processes, possibly due to modifications in Pt electronic structure induced by PPh_3 and Au. With a lower phase angle and peak frequencies of Pt_6 NC/C (71° and 1.894 Hz) and Au@Pt_6 NC/C (61° and 1.894 Hz) compared to Pt/C (78° and 1.079 Hz) in the Bode plot (Figure S15, Supporting

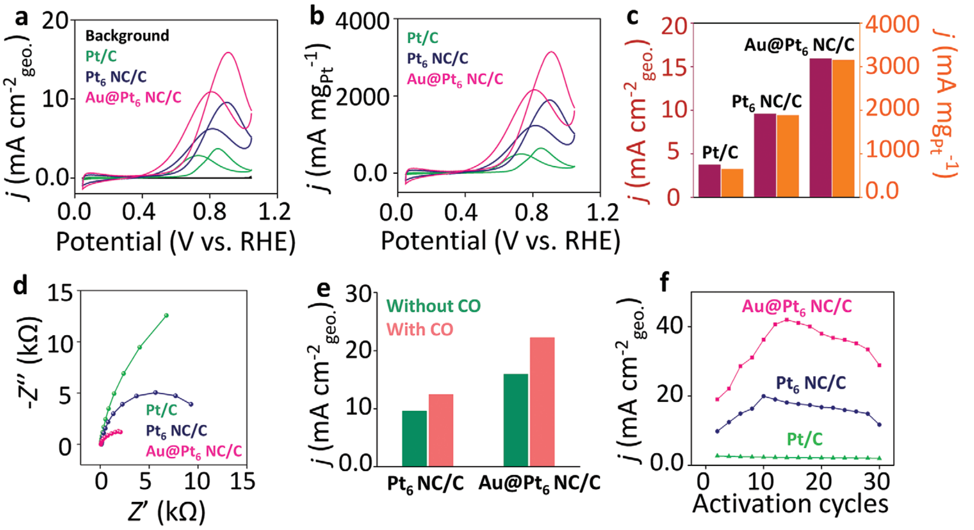

Figure 5. *i*R-corrected MOR curves of the Pt/C, Pt_6 NC/C, and Au@Pt_6 NC/C a) geometric area and b) Pt-mass normalized. c) Comparison of specific activities and mass activities of Pt/C, Pt_6 NC/C, and Au@Pt_6 NC/C. d) EIS Nyquist plot of Pt/C, Pt_6 NC/C, and Au@Pt_6 NC/C at 400 mV. e) Response of Pt/C, Pt_6 NC/C, and Au@Pt_6 NC/C toward the intentional CO poisoning in 0.1 м H_2SO_4 and 0.1 м Methanol. f) Stability test of Pt/C, Pt6 NC/C, and Au@Pt_6 NC/C.

Information) shows faster electron transfer kinetics and shorter electron lifetime.[15] The overpotential-dependent EIS performance was studied during MOR processes (Figures S16–S18, Supporting Information). From 0.30 to 0.40 $V_{Ag/AgCl}$, a decrease in R_{ct} was observed due to methanol oxidation to CO on the surface. Subsequently, between 0.45 and 0.55 $V_{Ag/AgCl}$, an increase in R_{ct} was noticed in consistence with sluggish removal of CO_{ads} aided by OH (Langmuir–Hinshelwood mechanism). From 0.60 to 0.80 $V_{Ag/AgCl}$, impedance appeared in the second and third quadrants of the Nyquist plot with an abrupt jump in the phase angle, which is attributed to faster oxidation of CO by OH thereby increasing the availability of free-Pt sites. In Au@Pt_6 NC/C, the Au atom is inert towards MOR in an acidic electrolyte. This suggests that catalytic reactions would proceed on the PtAu ensemble potentially achieving enhanced MOR activity due to electronic effect and CO tolerance facilitated by Au and PPh_3.

The chronoamperometric (CA) MOR stability test was conducted at 0.65 $V_{Ag/AgCl}$ (Figure S19, Supporting Information) under quiescent conditions for 4000 s. Notably, Pt_6 NC/C and Au@Pt_6 NC/C maintained their size distribution after the stability tests, while aggregation occurred in Pt/C (Figure S20a–c, Supporting Information). To further illustrate the CO tolerance, we recorded MOR both in the presence of CO in the electrolytes. The CV reveals the preferential oxidation of CO on Pt/C over MOR, while the MOR is predominant in both Pt_6 NC/C and Au@Pt_6 NC/C emphasizing their superior CO tolerance (Figure S21a–c, Supporting Information). In comparison to the MOR current density (j_{MOR}) without CO, the Pt_6 NC/C and Au@Pt_6 NC/C exhibited increased j_{MOR} by 1.27 and 1.40 times in the presence of CO with methanol (Figure 5e). This increment is attributed to the oxidation of methanol and CO together. The surface reactivity and stability under CV conditions for MOR was studied intermittently after activation cycles in methanol-free electrolytes (Figure 5f). The j_{MOR} increased as the cycle number was raised to ten cycles for Pt_6 NC/C (Figure S22b, Supporting Information) and 14 cycles for Au@Pt_6 NC/C (Figure S22c, Supporting Information) and declined slightly up to 25 cycles. The increase in j_{MOR} is attributed to the surface roughening of the catalyst associated with the removal of PPh_3 molecules and exposure of Pt sites. However, Au@Pt_6 NC/C exhibited better performance due to the stabilization of Pt by Au. The j_{MOR} of Pt/C declined from the first activation cycles, which is in agreement with the previous studies (Figure S22a, Supporting Information).[16]

To study the impact of the anodic potential limit (0.8 to 1.4 $V_{Ag/AgCl}$) on the MOR, CVs were recorded (Figure S23a–c, Supporting Information). The forward peak potential, E_f was constant and the forward peak current density, j_f scaled proportionally with anodic potential limits. A consistent negative shift in the backward peak potential (E_b) relative to the constant E_f occurred as the anodic potential limit increased in all the catalysts, indicating thicker Pt oxide (Figure S23d, Supporting Information). The Pt/C shows a decrease in backward peak current density (j_b) with increasing anodic potential limits due to reduced free-Pt sites as the surface would be covered with more oxides. Pt_6 NC/C displayed an initial decline followed by an increase in j_b as the anodic potential limit increased. The Au@Pt_6 NC/C exhibited a similar trend but with enhanced j_b. The attainment of higher j_b at lower anodic potentials resulted from the stable Pt_6 NC/C and Au@Pt_6 NC/C. The subsequent decrease in j_b is hypothesized to be due to PPh_3 removal, Au dissolution, and Pt oxide formation. The re-escalation of j_b is possibly due to the NC degradation and coalescence to larger NPs. All these steps resulted in a valley-like j_b trend revealing the intrinsic reactivity of the NCs. The valley with lower reactivity is named a "*Death Valley of Reactivity*".

3. Conclusion

In summary, we demonstrated the grafting of Au atoms on $Pt_6(PPh_3)_4Cl_5$ NCs using CO_{ads}, possibly the first molecular adsorbate-based self-termination process. The utilization of

CO_{ads} as a reducing and stabilizing agent is akin to the galvanic replacement of less-noble metals to obtain monolayer catalysts. This strategy enabled a surface structure with PtAu ensemble exhibiting enhanced MOR and CO tolerance. In addition to possible electronic interactions, the partial blocking of Pt-sites by Au for CO adsorption is the reason for higher MOR reactivity. The unusual variation in the j_b of MOR while increasing the anodic potentials revealed the intrinsic reactivity of the NCs in the presence of Au and PPh_3. In view of lowering noble metal utilization in electrocatalysts, our method offers a new vista for atomic-level surface modification on NCs for electrocatalysis.

4. Experimental Section

Reagents and Materials: All the chemicals and solvents were analytical grade and were used without any further purification. Hexachloroplatinic acid hexahydrate ($H_2PtCl_6{\cdot}6H_2O$), nafion solution (≈5%), sodium perchlorate ($NaClO_4$), perchloric acid ($HClO_4$), lead perchlorate ($Pb(ClO_4)_2$), sulfuric acid (H_2SO_4), ethanol, and toluene were purchased from Sigma-Aldrich. Commercial Pt/C (20%) catalyst was purchased from Alfa Aesar, Triphenylphosphine (PPh_3) and borane-*tert*-butylamine complex (TBAB) were purchased from TCI India. Carbon black (Vulcan XC-72R) was purchased from Cabot Carbon. All the experimental studies have been carried out using Milli-Q water.

Instrumentation and Characterization: UV–vis absorption spectra of NC were recorded on a VARIAN Cary 500 Scan spectrometer. High-resolution transmission electron microscopy (HAADF-TEM) images, STEM images, and elemental maps were recorded on an FEI Talos F200S (200 kV) transmission electron microscope. XPS spectra were recorded using a Thermo Scientific ESCALAB 250Xi (XR6 Micro-focused Monochromator, Al K_α). The mass spectrum of NC was recorded using Bruker Microflex matrix-assisted laser desorption ionization time-of-flight (MALDI-TOF) mass spectrometry. The ionization of molecules was achieved using Nd: YAG laser ($\lambda = 266$ nm). A standard solution of the matrix was prepared by dissolving 10 mg DCTB in 500 µL ethanol. NC solution was prepared at a ratio of 1 mg in 100 µL ethanol. Different compositions of matrix and NC solution were tried to optimize the well-resolved spectrum. All electrochemical experiments were conducted with an electrochemical workstation (model VSP-200; BioLogic workstation).

Synthesis of [$Pt_6(PPh_3)_4Cl_5$] NCs: [$Pt_6(PPh_3)_4Cl_5$] NCs were synthesized according to the procedure reported in the literature with substantial modification.[12] To a solution of TPP (32.75 mg/2.5 mL toluene), $H_2PtCl_6{\cdot}6H_2O$ (48.75 mg/5 mL H_2O) and 55 mL of ethanol were added under slow stirring at room temperature. Then, TBAB (4.35 mg/0.5 mL ethanol; 0.5 mol equivalents w.r.t. $H_2PtCl_6{\cdot}6H_2O$) was added while stirring at the same speed. The color gradually became dark brown and the solution was kept stirring for 3 h to get Pt_6 NCs. This dark brown precipitate was collected by centrifuging at 3000 rpm.

Synthesis of [$Pt_6(PPh_3)_4Cl_5$]/C: Ten milligram of carbon black (Vulcan XC-72R) was first dispersed in 50 mL of ethanol by sonicating and stirring for 2 h. Pt_6 NC/C with 10 wt% of Pt_6 NC loading was prepared by adding dispersion of $Pt_6(PPh_3)_4Cl_5$ (1 mg) NC in 1 mL of ethanol to the above solution. The dispersion kept stirring for another 6–8 h to get a uniform distribution of Pt_6 NC on carbon black. The final product was collected by centrifuging at 6000 rpm and dried at room temperature.

Au Grafting of Pt_6 NC/C: The process of Au grafting on Pt_6 NC/C was carried out through a chemical reduction approach using CO_{ads} as the reducing agent. A glassy carbon electrode was employed where Pt_6 NC/C was uniformly drop-casted (5 µg cm^{-2}). Through chronoamperometry, the CO was adsorbed on the surface of Pt_6 NC/C purging CO through the cell for 10 min. While keeping the working electrode at a constant potential of -0.20 $V_{Ag/AgCl}$ in 0.1 м H_2SO_4. Following this, the Pt_6 NC/C-CO_{ads} on the GCE were meticulously rinsed with ultrapure water. Next, the Au grafting process on the Pt_6 NC/C-CO_{ads} was conducted by immersing the electrode in a 0.1 mм $HAuCl_4$ solution at room temperature for 2 min. This step led to the formation of Au@Pt_6 NC/C on the electrode surface by reducing Au^{3+} to Au^0 by CO_{ads}. The resulting Au@Pt_6 NC/C was extensively washed with ultrapure water to eliminate any excess $HAuCl_4$ solution. The Pt_6 NC/C and the Au-grafted Au@Pt_6 NC/C were subsequently utilized for electrochemical studies.

Electrochemical Measurements: All the electrochemical studies were conducted in a biologic electrochemical workstation (BioLogic VSP-200 workstation) with a conventional three-electrode system at room temperature. To prepare the working electrode, the Pt_6 NC/C and commercial Pt/C (20 wt% of Pt) catalyst inks were prepared as described below: First, 2 mg (Pt_6 NC/C) and 0.5 mg (Pt/C) of each catalyst were dispersed into 375 µL of H_2O, 100 µL of isopropyl alcohol (IPA), and 25 µL of Nafion (5 wt%), then the dispersion was sonicated for 30 min to prepare a homogeneous catalyst ink. Then 2 µL of the catalyst ink was drop-caste on a glassy carbon electrode (GCE) of 3 mm diameter to get a catalyst loading of ca. 5 µg cm^{-2} for commercial Pt/C and Pt_6 NC/C, respectively. The MOR experiments were carried out in a standard three-electrode system with the GCE, an Ag/AgCl with 3 м KCl, and a Pt wire as the working, reference, and counter electrode, respectively. Before catalyst deposition, GCE was initially cleaned by polishing with alumina powder of grade, 0.05 µm followed by washing and sonication in Milli-Q water for 5 min. A reversible hydrogen electrode (RHE) potential was measured in the same electrolyte Pt/C coated GC electrode as the working electrode and corrected the potential from the Ag/AgCl (3 м KCl) reference electrode to the RHE scale.

Pre-Activation of Catalyst: Before any electrochemical measurements, the electrocatalyst drop-cast on GCE was activated by CV cycling in N_2 saturated 0.1 м H_2SO_4 solution between the potentials 0.05 to 1.05 V_{RHE} at 100 mV s^{-1}, for about two cycles of NCs and 20 cycles for Pt/C.

MOR Electrocatalysis: MOR CV measurements were performed in deaerated 1 м methanol and 0.1 м H_2SO_4 in the potential range of 0.0–1.5 V_{RHE} at 50 mV s^{-1}.

Pb-UPD Measurements: The Pb-UPD experiment involved cyclic voltammetry in a deaerated solution containing 0.1 м $NaClO_4$ and 0.01 м $HClO_4$ with 1 mм $Pb(ClO_4)_2$ solution. A constant potential of -0.42 V was maintained for 60 s to facilitate underpotential deposition. Subsequently, the cyclic voltammetric curve was recorded from -0.42 to $+0.3$ $V_{Ag/AgCl}$ at 20 mV s^{-1}. Before the measurements, the electrolytes underwent deaeration by subjecting them to N_2 bubbling for 20 min. The traces of oxygen in the nitrogen were scavenged by passing the nitrogen through an alkaline pyrogallol scrubber before purging in the electrochemical cell.

EIS Measurements: EIS was also performed using conventional three-electrode systems for MOR at different potentials. Before EIS, the equilibrium state was achieved by inducing each potential. After the current reached the equilibrium state, EIS was conducted with a voltage amplitude of 5 mV and a frequency range of 100 kHz to 1 mHz and at ten points per decade. The EIS of MOR was recorded at different overpotentials such as 0.30, 0.35, 0.40, 0.45, 0.50, 0.55, 0.60, 0.65, 0.70, 0.75, and 0.80 $V_{Ag/AgCl}$.

CO Stripping Experiments: The CO stripping activity of commercial Pt/C and Pt_6 NC/C was performed after purging CO through the cell for 10 min while keeping the working electrode at a constant potential of -0.20 $V_{Ag/AgCl}$, followed by N_2 purging for 10 min by maintaining the same potential to remove the unbound and dissolved CO. The CO stripping voltammograms were recorded by scanning the potential from 0.0 to 1.2 V at 50 mV s^{-1}. Both background current was subtracted from the CV recorded from the same samples under similar conditions without CO adsorption.

Supporting Information

Supporting Information is available from the Wiley Online Library or from the author.

Acknowledgements

C.J. thanks the Department of Science & Technology for funding through the SHRI scheme (DST/TDT/SHRI-42/2021). E.S.S. thanks the Department of Science and Technology (DST) for the Promotion of University Research and Scientific Excellence grant (PURSE;SR/PURSE/2023/191).

P.M. thanks the Council of Scientific and Industrial Research (CSIR) India for a Senior Research Fellowship through the National Eligibility Test. The authors thank the Central Instrumentation Facility (CIF), CSIR-CECRI, for Instrumentation support. CSIR-CECRI Ethics and Scientific Vigilance Committee Reference Number: CECRI/PESVC/Pubs/2024-31.

Conflict of Interest

The authors declare no conflict of interest.

Author Contributions

The project was conceived and supervised by C.J. Synthesis and characterization of the nanocluster was executed by P.M. The electrochemical experiments were performed and the manuscript was drafted by P.M. The manuscript was written through the contributions of P.M., E.S.S., and C.J. All authors have approved to the final version of the manuscript.

Data Availability Statement

The data that support the findings of this study are available from the corresponding author upon reasonable request.

Keywords

AuPt, electro-catalyst, methanol electrooxidation, precision nanoclusters, self-termination

Received: March 13, 2024
Revised: June 15, 2024
Published online:

---

[1] a) H. A. Gasteiger, N. Markovic, P. N. Ross, E. J. Cairns, *J. Phys. Chem.* **1993**, *97*, 12020; b) V. R. Stamenkovic, B. S. Mun, M. Arenz, K. J. J. Mayrhofer, C. A. Lucas, G. Wang, P. N. Ross, N. M. Markovic, *Nat. Mater.* **2007**, *6*, 241; c) H. A. Gasteiger, N. Markovic, P. N. Ross, E. J. Cairns, *J. Phys. Chem.* **1994**, *98*, 617; d) J. K. Nørskov, T. Bligaard, J. Rossmeisl, C. H. Christensen, *Nat. Chem.* **2009**, *1*, 37; e) W. Yu, M. D. Porosoff, J. G. Chen, *Chem. Rev.* **2012**, *112*, 5780.

[2] Z. L. Wang, *Science* **2007**, *316*, 732.

[3] a) J. Zhang, K. Sasaki, E. Sutter, R. R. Adzic, **2007**, *315*, 220; b) S. R. Brankovic, J. X. Wang, R. R. Adžić, *Surf. Sci.* **2001**, *474*, L173 ; c) D. Wang, H. L. Xin, H. Wang, Y. Yu, E. Rus, D. A. Muller, F. J. DiSalvo, H. D. Abruña, *Chem. Mater.* **2012**, *24*, 2274; d) C. Xu, Y. Zhang, L. Wang, L. Xu, X. Bian, H. Ma, Y. Ding, *Chem. Mater.* **2009**, *21*, 3110; e) G. Zhang, Y. Kuang, L. Liu, Y. Cui, J. Chen, H. Zhou, *Electrochem. Commun.* **2010**, *12*, 1233; f) Q. Wu, Y. Li, H. Xian, C. Xu, L. Wang, Z. Chen, *Nanotechnology* **2013**, *24*, 025501; g) P. Strasser, S. Kühl, *Nano Energy* **2016**, *29*, 166; h) N. Hodnik, C. Jeyabharathi, J. C. Meier, A. Kostka, K. L. Phani, A. Recnik, M. Bele, S. Hocˇevar, M. Gabersˇček, K. J. Mayrhofer, *Phys. Chem. Chem. Phys.* **2014**, *16*, 13610; i) L. J. J. Mayrhofer, V. Juhart, K. Hartl, M. Hanzlik, M. Arenz, *Angew. Chem., Int. Ed.* **2009**, *48*, 3529.

[4] L. Liang, Q. Feng, X. Wang, J. Hübner, U. Gernert, M. Heggen, L. Wu, T. Hellmann, J. P. Hofmann, P. Strasser, *Angew. Chem., Int. Ed.* **2023**, *62*, 202218039.

[5] J. Suntivich, Z. Xu, C. E. Carlton, J. Kim, B. Han, S. W. Lee, N. Bonnet, N. Marzari, L. F. Allard, H. A. Gasteiger, K. Hamad-Schifferli, Y. Shao-Horn, *J. Am. Chem. Soc.* **2013**, *135*, 7985.

[6] Z. Li, B. Li, Y. Hu, S. Wang, C. Yu, *Mater. Adv.* **2022**, *3*, 779.

[7] a) S. Yamazoe, K. Koyasu, T. Tsukuda, *Acc. Chem. Res.* **2014**, *47*, 816; b) I. Chakraborty, T. Pradeep, *Chem. Rev.* **2017**, *117*, 8208; c) R. Jin, C. Zeng, M. Zhou, Y. Chen, *Chem. Rev.* **2016**, *116*, 10346; d) R. Jin, *Nanoscale* **2015**, *7*, 1549; e) H. Häkkinen, *Chem. Soc. Rev.* **2008**, *37*, 1847; f) G. SchmM, *Chem. Rev.* **1992**, *92*, 1709; g) R. L. Whetten, J. T. Khoury, M. M. Alvarez, S. Murthy, I. Vezmar, Z. L. Wang, P. W. Stephens, C. L. Cleveland, W. D. Luedtke, U. Landman, *Adv. Mater.* **1996**, *8*, 428; h) J. F. Parker, C. A. Fields-Zinna, R. W. Murray, *Acc. Chem. Res.* **2010**, *43*, 1289; i) C. Jeyabharathi, S. Senthil Kumar, G. V. M. Kiruthika, K. L. N. Phani, *Angew. Chem., Int. Ed.* **2010**, *49*, 2925.

[8] a) L. Sumner, N. A. Sakthivel, H. Schrock, K. Artyushkova, A. Dass, S. Chakraborty, *J. Phys. Chem. C* **2018**, *122*, 24809; b) D. R. Kauffman, D. Alfonso, C. Matranga, H. Qian, R. Jin, *J. Am. Chem. Soc.* **2012**, *134*, 2333; c) S. Li, A. V. Nagarajan, X. Du, Y. Li, Z. Liu, D. R. Kauffman, G. Mpourmpakis, R. Jin, *Angew. Chem., Int. Ed.* **2022**, *61*, 202211771; d) H. Seong, V. Efremov, G. Park, H. Kim, J. S. Yoo, D. Lee, *Angew. Chem., Int. Ed.* **2021**, *60*, 14563; e) S. Zhao, R. Jin, H. Abroshan, C. Zeng, H. Zhang, S. D. House, E. Gottlieb, H. J. Kim, J. C. Yang, R. Jin, *J. Am. Chem. Soc.* **2017**, *139*, 1077; f) W. Chen, S. Chen, *Angew. Chem.* **2009**, *121*, 4450; g) K. Kwak, W. Choi, Q. Tang, M. Kim, Y. Lee, D. Jiang, D. Lee, *Nat. Commun.* **2017**, *8*, 14723; h) W. Choi, G. Hu, K. Kwak, M. Kim, D. Jiang, J.-P. Choi, D. Lee, *ACS Appl. Mater. Interfaces* **2018**, *10*, 44645; i) Y. Li, S. Li, A. V. Nagarajan, Z. Liu, S. Nevins, Y. Song, G. Mpourmpakis, R. Jin, *J. Am. Chem. Soc.* **2021**, *143*, 11102; j) S. Li, D. Alfonso, A. V. Nagarajan, S. D. House, J. C. Yang, D. R. Kauffman, G. Mpourmpakis, R. Jin, *ACS Catal.* **2020**, *10*, 12011; k) S. Li, A. V. Nagarajan, D. R. Alfonso, M. Sun, D. R. Kauffman, G. Mpourmpakis, R. Jin, *Angew. Chem., Int. Ed.* **2021**, *60*, 6351; l) D. Eguchi, M. Sakamoto, T. Teranishi, *Chem. Sci.* **2018**, *9*, 261; m) S. Li, A. V. Nagarajan, Y. Li, D. R. Kauffman, G. Mpourmpakis, R. Jin, *Nanoscale* **2021**, *13*, 2333; n) J. Wang, F. Xu, Z. Wang, S. Zang, T. C. W. Mak, *Angew. Chem., Int. Ed.* **2022**, *61*, 202207492; o) Y. Sun, X. Liu, K. Xiao, Y. Zhu, M. Chen, *ACS Catal.* **2021**, *11*, 11551.

[9] P. Mymoona, J. V. Rival, Nonappa, E. S. Shibu, *Small* **2023**, *20*, 2308610.

[10] a) C. N. Kostelansky, J. J. Pietron, M.-S. Chen, W. J. Dressick, K. E. Swider-Lyons, D. E. Ramaker, R. M. Stroud, C. A. Klug, B. S. Zelakiewicz, T. L. Schull, *J. Phys. Chem. B* **2006**, *110*, 21487; b) A. L. Ankudinov, J. J. Rehr, J. J. Low, S. R. Bare, *J. Chem. Phys.* **2002**, *116*, 1911.

[11] a) J. C. Meier, C. Galeano, I. Katsounaros, J. Witte, H. J. Bongard, A. A. Topalov, C. Baldizzone, S. Mezzavilla, F. Schüth, K. J. J. Mayrhofer, *Beilstein J. Nanotechnol.* **2014**, *5*, 44; b) M. Bogar, Y. Yakovlev, D. J. S. Sandbeck, S. Cherevko, I. Matolínová, H. Amenitsch, I. Khalakhan, *ACS Catal.* **2021**, *11*, 11360; c) I. Martens, R. Chattot, J. Drnec, *J. Power Sources* **2022**, *521*, 230851; d) S. Cherevko, G. P. Keeley, S. Geiger, A. R. Zeradjanin, N. Hodnik, N. Kulyk, K. J. J. Mayrhofer, *ChemElectroChem* **2015**, *2*, 1471; e) J. C. Meier, C. Galeano, I. Katsounaros, A. A. Topalov, A. Kostka, F. Schüth, K. J. J. Mayrhofer, *ACS Catal.* **2012**, *2*, 832; f) M. Gatalo, P. Jovanovič, G. Polymeros, J.-P. Grote, A. Pavlišič, F. Ruiz- Zepeda, V. S. Šelih, M. Šala, S. Hočevar, M. Bele, K. J. J. Mayrhofer, N. Hodnik, M. Gaberšček, *ACS Catal.* **2016**, *6*, 1630; g) X. Xie, V. Briega-Martos, R. Farris, M. Dopita, M. Vorokhta, T. Skála, I. Matolínová, K. M. Neyman, S. Cherevko, I. Khalakhan, *ACS Appl. Mater. Interfaces* **2023**, *15*, 1192.

[12] X. Wang, L. Zhao, X. Li, Y. Liu, Y. Wang, Q. Yao, J. Xie, Q. Xue, Z. Yan, X. Yuan, W. Xing, *Nat. Commun.* **2022**, *13*, 1596.

[13] M. A. Hewitt, H. Hernández, G. E. Johnson, *J. Am. Soc. Mass Spectrom.* **2021**, *32*, 237.

[14] Y. Yu, Z. Luo, D. M. Chevrier, D. T. Leong, P. Zhang, D. Jiang, J. Xie, *J. Am. Chem. Soc.* **2014**, *136*, 1246.

[15] T. Huang, S. Mao, G. Zhou, Z. Zhang, Z. Wen, X. Huang, S. Ci, J. Chen, *Nanoscale* **2015**, *7*, 1301.

[16] C. Jeyabharathi, J. Mathiyarasu, K. L. N. Phani, *J. Appl. Electrochem.* **2009**, *39*, 45.